

# The ternary Ni–Al–Co embedded-atom-method potential for $\gamma/\gamma'$ Ni-based single-crystal superalloys: Construction and application\*

Du Jun-Ping(杜俊平)<sup>a)</sup>, Wang Chong-Yu(王崇愚)<sup>a)b)c)†</sup>, and Yu Tao(于涛)<sup>a)</sup>

<sup>a)</sup> Central Iron and Steel Research Institute, Beijing 100081, China

<sup>b)</sup> Department of Physics, Tsinghua University, Beijing 100084, China

<sup>c)</sup> The International Center for Materials Physics, Chinese Academy of Sciences, Shenyang 110016, China

(Received 31 July 2013; revised manuscript received 23 September 2013; published online 24 January 2014)

An Ni–Al–Co system embedded-atom-method potential is constructed for the  $\gamma(\text{Ni})/\gamma'(\text{Ni}_3\text{Al})$  superalloy based on experiments and first-principles calculations. The stacking fault energies (SFEs) of the Ni(Co, Al) random solid solutions are calculated as a function of the concentrations of Co and Al. The calculated SFEs decrease with increasing concentrations of Co and Al, which is consistent with the experimental results. The embedding energy term in the present potential has an important influence on the SFEs of the random solid solutions. The cross-slip processes of a screw dislocation in homogenous Ni(Co) solid solutions are simulated using the present potential and the nudged elastic band method. The cross-slip activation energies increase with increasing Co concentration, which implies that the creep resistance of  $\gamma(\text{Ni})$  may be improved by the addition of Co.

**Keywords:** interatomic interaction potential, embedded-atom method, Ni-based single-crystal superalloys

**PACS:** 34.20.Cf, 61.72.Nn

**DOI:** 10.1088/1674-1056/23/3/033401

## 1. Introduction

Ni-based single-crystal superalloys have been widely applied in the manufacture of gas turbine blades due to the alloys' superior high-temperature strength and creep resistance.<sup>[1]</sup> The Ni-based single-crystal superalloys consist of two phases: the face-centered cubic (fcc)  $\gamma$  phase and the ordered  $\gamma'$  ( $L1_2$ ) phase. The  $\gamma$  and  $\gamma'$  phases contain more than ten elements, such as Ni, Al, Cr, Co, Mo, Re, and Ru. Some of the elements, such as Cr, Co, Ru, Mo, and Re, prefer to distribute in the  $\gamma$  phase.<sup>[1]</sup> These elements play an important role in improving the mechanical properties of the superalloys. The Co element has been used in the first, second, third, and fourth generations of superalloys because the mechanical properties of the  $\gamma$  phase are improved by the addition of Co. The addition of Co reduces the stacking fault energy (SFE) of the Ni–Co alloy. The minimum creep rate of the Ni–Co alloy is proportional to the  $n$ -th power of the SFE; thus the creep resistance is improved.<sup>[1]</sup> Lowering the SFE by alloying with Co also promotes primary creep under high-stress and low-temperature conditions, such as 500 Mpa and 750 °C for the CMSX-4 superalloy.<sup>[2]</sup> The resistance of the superalloys to oxidation, corrosion, and sulfidation is also improved by the addition of Co.<sup>[3]</sup> Metals of Co and Ni have similar densities, so Co-based superalloys have been developed for high-temperature applications.<sup>[4]</sup>

Molecular dynamics (MD) simulations have been used to study the effects of the solute elements on the mechan-

ical properties of the superalloys.<sup>[5–9]</sup> Empirical interatomic interaction potentials, such as the embedded-atom method (EAM),<sup>[10,11]</sup> should be constructed for the MD simulations. The empirical potentials can be obtained by different methods, such as fitting experimental or first-principles databases of materials,<sup>[12–14]</sup> and the lattice inversion method.<sup>[15–19]</sup> The potentials of Co have been proposed by some authors.<sup>[20–23]</sup> To continue our previous work on the construction of multi-element potentials, the EAM potential of Co is constructed based on the same formula used for the Ni–Al–Re EAM potential.<sup>[24]</sup>

This paper is arranged as follows. The construction of the present Ni–Al–Co potential is presented in Section 2. The application and discussion of the potential are presented in Section 3, and the final section gives a summary.

## 2. Construction of the potentials

### 2.1. The potentials model

In the EAM scheme,<sup>[10,11]</sup> the total energy of the  $N$  atoms is represented as

$$E_{\text{tot}} = \sum_i F_i(\rho_i) + \sum_{i>j} \phi(r_{ij}), \quad (1)$$

where  $F(\rho_i)$  is the embedding energy of atom  $i$ , and  $\phi(r_{ij})$  is the pair potential between atoms  $i$  and  $j$ . The host electron density  $\rho_i$  is assumed to be a linear superposition of the atomic

\*Project supported by the National Basic Research Program of China (Grant No. 2011CB606402) and the National Natural Science Foundation of China (Grant No. 51071091).

†Corresponding author. E-mail: cywang@mail.tsinghua.edu.cn

© 2014 Chinese Physical Society and IOP Publishing Ltd

<http://iopscience.iop.org/cpb> <http://cpb.iphy.ac.cn>

electron density  $f(r_{ij})$ , i.e.,

$$\rho_i = \sum_j f(r_{ij}). \quad (2)$$

The embedding energy function  $F(\rho)$ , atomic electron density  $f(r_{ij})$ , and pair potential  $\phi(r_{ij})$  are determined by the formulas in our previous work.<sup>[24]</sup> The monoatomic potentials for Ni and Al and the pair potential for Ni–Al have been constructed in previous work.<sup>[24]</sup> For the Ni–Al–Co potentials, we just need to fit the monoatomic potential for Co and the pair potentials for Ni–Co and Al–Co.

The embedding energy  $F(\rho)$  of the monoatomic potential for Co is parameterized as<sup>[25]</sup>

$$F(\rho) = -F_0 \left\{ 1 - \ln \left( \frac{\rho}{\rho_e} \right)^n \right\} \left( \frac{\rho}{\rho_e} \right)^n, \quad (3)$$

where  $F_0 = E_c - E_v^f$ ,  $E_c$  and  $E_v^f$  are the cohesive energy and the vacancy formation energy, respectively,  $n$  is an adjustable parameter, and  $\rho_e$  is the equilibrium host electron density. The atomic electron density is parameterized as

$$f(r) = s \tilde{f}(r) \psi \left( \frac{r - r_c}{h} \right), \quad (4)$$

$$\tilde{f}(r) = f_e \exp[-\chi(r - r_e)], \quad (5)$$

with

$$\psi(x) = \begin{cases} \frac{x^4}{1+x^4}, & x < 0, \\ 0, & x \geq 0, \end{cases} \quad (6)$$

where  $s$ ,  $r_c$ , and  $h$  are adjustable parameters;  $f_e$ ,  $\chi$ , and  $r_e$  are obtained by fitting the radial electron density calculated by Dmol3;<sup>[26,27]</sup> and  $\Psi(x)$  is a cutoff function.<sup>[28]</sup>

The pair potentials for Co–Co, Ni–Co, and Al–Co are parameterized as

$$\phi_{AB}(r) = \{ \phi_{AB} - \gamma \exp[-\kappa(r/r_0 - 1)] \} \psi \left( \frac{r - r_c}{h} \right), \quad (7)$$

$$\phi_{AB} = -\alpha [1 + \beta(r/r_0 - 1)] \exp[-\beta(r/r_0 - 1)] + d_{AB}^A s_A \tilde{f}_A(r) / \rho_e^A + d_{AB}^B s_B \tilde{f}_B(r) / \rho_e^B, \quad (8)$$

where  $A = \text{Ni, Al, Co}$ ,  $B = \text{Co}$ , and  $r_0$  in  $\phi_{\text{CoCo}}(r)$  is the first-nearest neighbor of Co with a hexagonal close-packed (hcp) structure. The parameter  $n$  in  $F_{\text{Co}}(\rho)$  and the parameters  $\alpha$ ,  $\beta$ ,  $\gamma$ ,  $\kappa$ ,  $d_{\text{CoCo}}^{\text{Co}}$ ,  $h$ , and  $r_c$  in  $\phi_{\text{CoCo}}(r)$  are determined by fitting the experimental properties of hcp-Co. The parameter  $s_{\text{Co}}$  in  $f(r)$  and the parameters  $\alpha$ ,  $\beta$ ,  $\gamma$ ,  $\kappa$ ,  $r_0$ ,  $d_{AB}^A$ ,  $d_{AB}^B$ ,  $h$ ,  $r_c$  in  $\phi_{\text{NiCo}}(r)$  and  $\phi_{\text{AlCo}}(r)$  are given by fitting the first-principles data of virtual compounds.

## 2.2. Fitting the potential for Co

The properties used in the fitting of the potential for hcp-Co are the lattice parameters  $a$  and  $c$ , cohesive energy, elastic constants, vacancy formation energy, the Rose equation,

and the  $I_2$  SFE. The inner elastic constants<sup>[21,24,29,30]</sup> are included in the fitting of the elastic constants of Co. The parameters in the potential are given by minimizing the weighted mean square deviation between the calculated and experimental data. The optimized parameters are listed in Table 1. The  $I_2$  SFE is not directly included in the fitting because the SFE calculation needs the relaxed energy of the model containing the  $I_2$  stacking fault. In the process of optimizing potential parameters, some bad trial parameters make the fitting process time consuming. Because the energy of the fcc–hcp structural stability is closely related to the  $I_2$  SFE of hcp metals, the energy of the fcc–hcp structural stability is directly used in the fitting. The energy of the fcc–hcp structural stability is defined as

$$\Delta E_{\text{fcc-hcp}} = E_b^{\text{fcc}} - E_b^{\text{hcp}}, \quad (9)$$

where  $E_b^{\text{fcc}}$  and  $E_b^{\text{hcp}}$  are the binding energies per atom of fcc-Co and hcp-Co, respectively. The  $\Delta E_{\text{fcc-hcp}}$  used in the fitting is obtained by extrapolating from three sets of trial parameters, as shown in Fig. 1.

**Table 1.** The optimized values of the potential parameters of the present EAM potential for Co.

Parameter	Value	Parameter	Value
$f_e$	$3.31 \times 10^{-3}$	$\beta$	9.3735
$r_e/\text{\AA}$	2.50	$r_0/\text{\AA}$	2.4935
$\chi/\text{\AA}^{-1}$	2.7729	$\gamma/\text{eV}$	$1.4415 \times 10^{-1}$
$n$	$4.0148 \times 10^{-1}$	$\kappa$	3.0729
$d_{\text{CoCo}}^{\text{Co}}/\text{eV}$	$7.6368 \times 10^{-1}$	$h$	$9.0172 \times 10^{-1}$
$\alpha/\text{eV}$	$1.4900 \times 10^{-1}$	$r_c/\text{\AA}$	5.8996

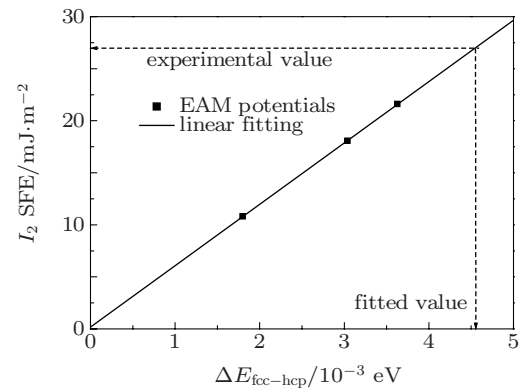


**Fig. 1.** The relationship between  $\Delta E_{\text{fcc-hcp}}$  and  $I_2$  SFE for three sets of trial potentials for Co (solid square symbols) and the linear fitting (line) used in the extrapolation of the fitted  $\Delta E_{\text{fcc-hcp}}$ .

## 2.3. Fitting the pair potentials for Ni–Co and Al–Co

The pair potentials for Ni–Co and Al–Co are obtained by fitting the first-principles data of virtual compounds consisting of Ni, Al, and Co atoms. The first-principles data include the lattice constants and the binding energies for the following ordered structures:  $L1_2\text{-Ni}_3\text{Co}$ ,  $D0_{19}\text{-Ni}_3\text{Co}$ ,  $D0_{22}\text{-Ni}_3\text{Co}$ ,  $B2\text{-NiCo}$ ,  $L1_2\text{-Co}_3\text{Ni}$ ,  $L1_2\text{-Co}_3\text{Al}$ ,  $D0_{19}\text{-Co}_3\text{Al}$ ,  $D0_{22}\text{-Co}_3\text{Al}$ ,

$B2$ -CoAl,  $L1_2$ -Al<sub>3</sub>Co, and  $L2_1$ -Ni<sub>2</sub>CoAl. In order to obtain the correct site preference of Co atoms in Ni<sub>3</sub>Al, the binding energies of models Ni<sub>24</sub>Al<sub>7</sub>Co and Ni<sub>23</sub>Al<sub>8</sub>Co are also included in the fitting. The models of Ni<sub>24</sub>Al<sub>7</sub>Co and Ni<sub>23</sub>Al<sub>8</sub>Co are obtained by replacing an Al atom and an Ni atom in a  $2 \times 2 \times 2$  Ni<sub>3</sub>Al supercell with a Co atom, respectively. The equilibrium lattice parameters of the structures listed above are determined by performing a series of total energy calculations with different lattice constants, except for the  $D0_{19}$  and  $D0_{22}$  structures. The  $D0_{19}$  and  $D0_{22}$  structures are fully relaxed with respect to the unit cell volume, shape, and atomic positions. Note that the binding energies in the first-principles database are scaled by the requirement that the formation heat calculated using the binding energies of Ni, Al and Co from the present monoatomic metal potentials is equal to that from the first-principles calculations. The following expression is used to estimate the formation heat per atom of a supercell:<sup>[31]</sup>

$$H = [E_i(n, m, l) - n \times E_b(\text{Ni}) - m \times E_b(\text{Al}) - l \times E_b(\text{Co})] / (n + m + l), \quad (10)$$

where  $E_i(n, m, l)$  is the binding energy of the supercell with  $n$  Ni atoms,  $m$  Al atoms, and  $l$  Co atoms.  $E_b(\text{Ni})$ ,  $E_b(\text{Al})$ , and  $E_b(\text{Co})$  are the binding energies of Ni, Al, and Co, respectively. Furthermore, two models of Co atoms located at the  $\gamma(\text{Ni})/\gamma'$  (Ni<sub>3</sub>Al) interface (see Fig. 1 of Ref. [32]) are used in the fitting. The binding energy difference between the models,  $\Delta E_b^{\gamma(\text{Co})/\gamma'(\text{Co})} = E_b^{\gamma/\gamma'(\text{Co})} - E_b^{\gamma(\text{Co})/\gamma'}$ , is used in the fitting of the potentials, where  $E_b^{\gamma/\gamma'(\text{Co})}$  and  $E_b^{\gamma(\text{Co})/\gamma'}$  are the binding energies for the models of Co located in the  $\gamma(\text{Ni})$  and  $\gamma'(\text{Ni}_3\text{Al})$  regions, respectively. The first-principles calculations are performed using the Vienna *ab-initio* simulation

package (VASP).<sup>[33,34]</sup> We employ the generalized gradient approximation (GGA) for the exchange correlation functional. All calculations are carried out in a spin-restricted mode in order to be consistent with the fitting of the Ni–Al–Re potential. The cutoff energy of the plane-wave basis set is set to 350 eV. The accuracy for electronic minimization is  $10^{-4}$  eV, and for ionic relaxation is  $10^{-3}$  eV.

The pair potential parameters for Ni–Co and Al–Co, and the parameter  $s_{\text{Co}}$  are given by minimizing the weighted mean square deviation between the calculated and the first-principles data. The optimized parameters are listed in Table 2. The lattice parameters and binding energies of the ordered structures, calculated with both VASP and the present potential, are listed in Table 3. It can be seen from Table 3 that the lattice parameters and the binding energies of the compounds calculated from the present EAM are in fair agreement with those from first-principles calculations. The pair potentials of Ni–Co and Al–Co are shown in Fig. 2, compared with the pair potential of Co–Co.

**Table 2.** The optimized values of the potential parameters of the pair potentials for Ni–Co and Al–Co, and  $s_{\text{Co}}$ .

Ni–Co		Al–Co	
Parameter	Value	Parameter	Value
$\alpha/\text{eV}$	$1.1452 \times 10^{-1}$	$\alpha/\text{eV}$	1.2783
$\beta$	8.6437	$\beta$	8.5789
$\gamma/\text{eV}$	$1.7595 \times 10^{-1}$	$\gamma/\text{eV}$	$-2.4237 \times 10^1$
$\kappa$	2.9149	$\kappa$	4.4245
$r_0/\text{\AA}$	2.4806	$r_0/\text{\AA}$	1.4441
$d_{\text{NiCo}}^{\text{Ni}}/\text{eV}$	1.3306	$d_{\text{AlCo}}^{\text{Al}}/\text{eV}$	-8.9779
$d_{\text{NiCo}}^{\text{Co}}/\text{eV}$	$1.2013 \times 10^{-2}$	$d_{\text{AlCo}}^{\text{Co}}/\text{eV}$	8.0876
$h/\text{\AA}^{-1}$	$6.8613 \times 10^{-1}$	$h/\text{\AA}^{-1}$	$4.1946 \times 10^{-1}$
$r_c/\text{\AA}$	5.4315	$r_c/\text{\AA}$	6.3593
$s_{\text{Co}}$	2.5592		

**Table 3.** The properties used in the fitting of the pair potentials for Ni–Co and Al–Co, as obtained from VASP calculations, compared here with the values obtained from the present potential.

Formula	Structure	Lattice constant/ $\text{\AA}$		binding energy/eV per atom	
		First-principles	Present EAM	First-principles	Present EAM
Ni <sub>3</sub> Co	$L1_2$	3.50	3.50	-4.40	-4.36
Ni <sub>3</sub> Co	$D0_{19}$	$a = 4.95, c/a = 0.82$	$a = 4.96, c/a = 0.80$	-4.38	-4.35
Ni <sub>3</sub> Co	$D0_{22}$	$a = 3.50, c/a = 2.00$	$a = 3.50, c/a = 2.00$	-4.40	-4.35
NiCo	$B2$	2.78	2.74	-4.25	-4.29
Co <sub>3</sub> Ni	$L1_2$	3.47	3.51	-4.37	-4.34
Co <sub>3</sub> Al	$L1_2$	3.54	3.54	-4.43	-4.43
Co <sub>3</sub> Al	$D0_{19}$	$a = 4.98, c/a = 0.82$	$a = 5.01, c/a = 0.81$	-4.42	-4.44
Co <sub>3</sub> Al	$D0_{22}$	$a = 3.57, c/a = 1.94$	$a = 3.54, c/a = 2.00$	-4.45	-4.44
CoAl	$B2$	2.86	2.86	-4.59	-4.27
Al <sub>3</sub> Co	$L1_2$	3.80	3.84	-3.89	-3.76
Ni <sub>2</sub> CoAl	$L2_1$	5.68	5.56	-4.48	-4.50
Ni <sub>24</sub> Al <sub>7</sub> Co	supercell $2 \times 2 \times 2$	3.56	3.56	-4.61	-4.61
Ni <sub>23</sub> Al <sub>8</sub> Co	supercell $2 \times 2 \times 2$	3.56	3.56	-4.63	-4.64
$\Delta E_b^{\gamma(\text{Co})/\gamma'(\text{Co})}$	supercell $3 \times 3 \times 4$	–	–	$0.96 \times 10^{-3}$	$1.05 \times 10^{-3}$

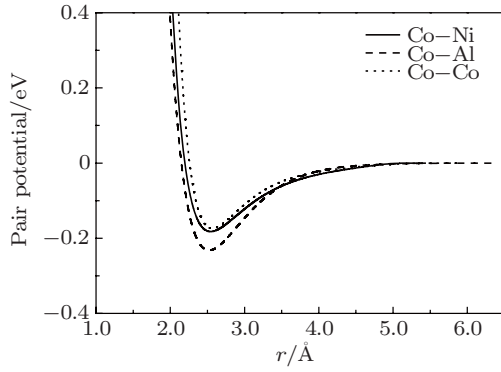


Fig. 2. The pair potentials for Ni-Co, Al-Co, and Co-Co.

### 3. Application and discussion

#### 3.1. Properties of hcp-Co

The properties of hcp-Co calculated with the present potential are listed in Table 4, in comparison with those from first-principles calculations or the experimental values. It can be seen from Table 4 that the lattice parameters, cohesive energy, and elastic constants calculated with the present potential are in excellent agreement with the experimental data. The structural stability energies of hcp-Co with respect to the fcc, body-centered cubic (bcc), simple cubic (sc), and diamond

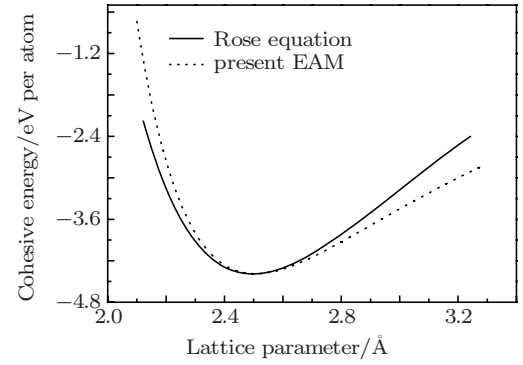
**Table 4.** The properties of Co calculated with the present EAM potential compared with the experimental data.

Property	Experiment or first-principles	Present EAM
$a/\text{\AA}$	2.497 <sup>a)</sup> <sup>b)</sup>	2.497
$c/a$	1.63 <sup>a)</sup> <sup>b)</sup>	1.63
$E_c/\text{eV}$	4.39 <sup>b)</sup> <sup>c)</sup>	4.39
Elastic constants/Mbar		
$C_{11}$	2.95 <sup>b)</sup> <sup>d)</sup>	2.93
$C_{12}$	1.59 <sup>b)</sup> <sup>d)</sup>	1.51
$C_{44}$	0.71 <sup>b)</sup> <sup>d)</sup>	0.70
$C_{33}$	3.35 <sup>b)</sup> <sup>d)</sup>	3.49
$C_{13}$	1.11 <sup>b)</sup> <sup>d)</sup>	1.10
Structural stabilities/eV per atom		
$\Delta E_{\text{fcc-hcp}}$	0.02 <sup>e)</sup>	$4.54 \times 10^{-3}$
$\Delta E_{\text{bcc-hcp}}$	0.10 <sup>e)</sup>	0.05
$\Delta E_{\text{sc-hcp}}$	0.77 <sup>e)</sup>	0.51
$\Delta E_{\text{diamond-hcp}}$	1.34 <sup>e)</sup>	0.99
Vacancy formation and migration energies/eV		
$E_v^f$	1.35 <sup>f)</sup>	1.35
$E_v^m$ (in the plane)		0.91
$E_v^m$ (out of the plane)		0.96
Stacking fault energies/ $\text{mJ}\cdot\text{m}^{-2}$		
$I_2$	27 <sup>g)</sup>	27
$I_1$		13
Surface energies/ $\text{mJ}\cdot\text{m}^{-2}$		
(0001)	2550 <sup>f)</sup>	1316
(1120)		1506

<sup>a)</sup>Ref. [36]; <sup>b)</sup>included in the fitting database; <sup>c)</sup>Ref. [37]; <sup>d)</sup>Ref. [38];

<sup>e)</sup>calculated with VASP; <sup>f)</sup>Ref. [39]; <sup>g)</sup>Ref. [40].

structures from VASP are calculated using a spin-unrestricted mode. The structure stability energies calculated from the present potential are lower than those from VASP. The vacancy formation energy calculated with the present potential is in excellent agreement with the experimental value. Vacancy migration in a basal plane is energetically preferred to vacancy migration out of the basal plane. The  $I_2$  SFE calculated with the present potential is in excellent agreement with the experimental data. The  $\Delta E_{\text{fcc-hcp}}$  calculated with the present potential is also consistent with the fitted value described in Subsection 2.2, so the fitting method described in Subsection 2.2 is effective. The  $I_1$  SFE calculated with the present potential is half of the  $I_2$  SFE, and the surface energies calculated with the present potential are lower than the experimental value. The equations of state calculated with the present EAM and the Rose equation<sup>[35]</sup> are shown in Fig. 3. It can be seen from Fig. 3 that the equation of state from the present EAM is in reasonable agreement with that from the Rose equation.


**Fig. 3.** Equations of state for Co calculated with the present EAM and the Rose equation.

#### 3.2. The effect of Co on the interface lattice misfit between $\gamma(\text{Ni})$ and $\gamma'(\text{Ni}_3\text{Al})$

The interface lattice misfit has an important influence on the creep properties of superalloys.<sup>[41,42]</sup> The addition of Co can decrease the lattice misfit between the  $\gamma$  and  $\gamma'$  phases.<sup>[43,44]</sup> A  $2 \times 2 \times 2$  supercell of fcc-Ni is used as the  $\gamma(\text{Ni})$  phase, and the Co-doped  $\gamma(\text{Ni}(\text{Co}))$  phase is constructed by replacing an Ni atom of the supercell with Co. Similarly, the Co-doped  $\gamma'(\text{Ni}_3(\text{Al}, \text{Co}))$  phase is constructed by replacing an Al atom of a  $2 \times 2 \times 2$  supercell of  $\gamma'(\text{Ni}_3\text{Al})$  with Co. The lattice misfit is defined as

$$\delta = 2 \frac{a'_\gamma - a_\gamma}{a'_\gamma + a_\gamma}, \quad (11)$$

where  $a_\gamma$  and  $a'_\gamma$  are the lattice parameters of the  $\gamma$  and  $\gamma'$  phases, respectively. The lattice parameters and lattice misfits calculated with the present potential and comparable first-principles results are listed in Table 5. It can be seen from Table 5 that the lattice parameters of  $\gamma(\text{Ni})$  and  $\gamma'(\text{Ni}_3\text{Al})$  are

decreased by the addition of 3.1 at.% Co. The interface lattice parameter is also decreased due to the addition of Co. The results from the EAM are in agreement with those from the first-principles calculations.

**Table 5.** The lattice parameters and lattice misfits of  $\gamma(\text{Ni})$ ,  $\gamma'(\text{Ni}_3\text{Al})$ , alloyed  $\gamma(\text{Ni}(\text{Co}))$ , and  $\gamma'(\text{Ni}_3(\text{Al},\text{Co}))$  derived from the present EAM and VASP.

	VASP <sup>a)</sup>		Present EAM	
	$a/\text{\AA}$	$\delta/\%$	$a/\text{\AA}$	$\delta/\%$
$\gamma(\text{Ni})$	3.515	1.50	3.520	1.33
$\gamma'(\text{Ni}_3\text{Al})$	3.568		3.567	
$\gamma(\text{Ni}(\text{Co}))$	3.513	1.36	3.518	1.16
$\gamma'(\text{Ni}_3(\text{Al},\text{Co}))$	3.561		3.559	

<sup>a)</sup> Ref. [45].

### 3.3. The effect of Co and Al on the SFE of the Ni(Co, Al) random solid solution

The SFE of  $\gamma(\text{Ni})$  can be decreased by the solute atoms, such as Co and Al. Although the steady-state creep rates of Ni alloys are strongly related to their SFEs, no systematic relationship has been established between the SFEs of alloys and the solute elements.<sup>[1]</sup> The relationship between the SFE of  $\gamma(\text{Ni})$  and the concentrations of Co and Al is calculated based on the present Ni–Al–Co potential. The concentrations of Co and Al are selected to be 3.1 at.%, 6.3 at.%, 9.4 at.%, and 12.5 at.%. These concentrations are selected in order to compare them with the results of the homogenous solid solutions in Subsection 3.4. The distributions of Co and Al atoms are fully random in the fcc-Ni lattice. The random solid solution models are created in a cubic cell with sizes  $10[\bar{1}\bar{1}2]a_0$ ,  $30[1\bar{1}0]a_0$ , and  $10[111]a_0$  along the  $x$ ,  $y$ , and  $z$  directions, respectively. Here,  $a_0$  is the lattice parameter of the random solid solution. The  $x$  and  $y$  directions of the cell have periodic boundary conditions and the  $z$  direction has a free boundary condition. The stacking fault is formed on the plane  $(0, 0, 5\sqrt{3}a_0)$ . The SFE of the Ni(Co, Al) random solid solution is calculated by  $E_{\text{sf}} = (E_2 - E_1)/S$ , where  $E_1$  and  $E_2$  are the minimized energies of the models without and with the stacking fault, respectively, and  $S$  is the area of the stacking fault. The size of the system in the  $z$  direction is large enough to neglect the influence of the surfaces on the SFE. For a set of concentrations of Co and Al, 20 random solid solutions are created with different sets of random numbers and the SFEs are calculated. The SFE of the random solid solution is given by calculating the average value of the 20 calculated SFEs. The SFEs as a function of the concentrations of Co and Al are shown in Fig. 4(a). The SFEs of the Ni-based solid solution can be expressed as a linear function of the concentrations of solutes by fitting the experimental results<sup>[46]</sup>

$$E_{\text{SF}}^{\text{alloy}} = E_{\text{SF}}^{\text{Ni}}(1 - 1.72c_{\text{Al}} - 0.96c_{\text{Co}} - 1.66c_{\text{Cr}} - 8.0 \times c_{\text{Ti}} - 1.66 \times c_{\text{Mo}} - Z_{\text{W}}),$$

$$Z_{\text{W}} = \begin{cases} 76.9 \times c_{\text{W}}, & c_{\text{W}} \leq 0.0065, \\ 0.5, & c_{\text{W}} > 0.0065, \end{cases}$$

where  $E_{\text{SF}}^{\text{alloy}}$ ,  $E_{\text{SF}}^{\text{Ni}}$ , and  $c_X$  are the SFE of the solid solution, the SFE of  $\gamma(\text{Ni})$ , and the atomic fraction of solute  $X$ , respectively. It can be seen from the experimental results that Co and Al can decrease the SFE of  $\gamma(\text{Ni})$  effectively. The calculated SFEs of the Ni(Co, Al) random solid solutions in Fig. 4(a) are fitted by a linear function of the concentrations of Co and Al. The fitting result is  $E_{\text{SF}}^{\text{alloy}} = E_{\text{SF}}^{\text{Ni}}(1 - 3.16c_{\text{Al}} - 2.48c_{\text{Co}})$ .

The SFE values of the Ni(Co, Al) solid solutions from both the experiments and the present potential decrease with increasing concentrations of Co and Al. Starting with the same concentrations of Co and Al, the SFE can be decreased more by adding Al than by adding Co based on the the linear function for the present potential, which is in agreement with the experimental results.<sup>[46]</sup> However, the coefficients of  $c_{\text{Co}}$  and  $c_{\text{Al}}$  in the linear function from the present potential are smaller than those from the experiments.<sup>[46]</sup> This may be because the Ni(Co, Al) solid solution in the present simulation is fully chemically disordered, while the solid solution in the experiments may be short-range ordered, such as the Ni(Al) solid solution.<sup>[47]</sup>

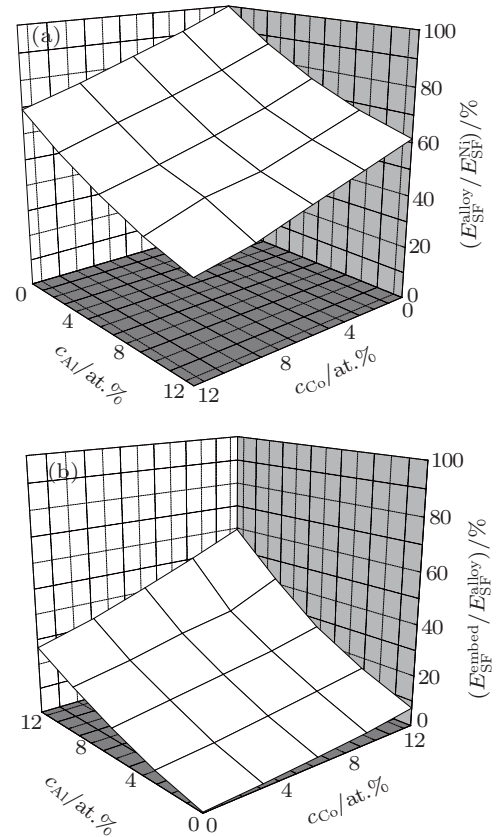


**Fig. 4.** (a) The stacking fault energies ( $E_{\text{SF}}^{\text{alloy}}$ ) of Ni(Co, Al) random solid solutions as a function of the concentrations of Co and Al calculated with the present potential, where  $E_{\text{SF}}^{\text{Ni}}$  is the SFE of  $\gamma(\text{Ni})$ . (b) The contributions of the embedding energy term ( $E_{\text{SF}}^{\text{embed}}$ ) to the stacking fault energies of the Ni(Co, Al) random solid solutions as a function of the concentrations of Co and Al calculated with the present potential.



The material properties calculated with the EAM are given by the contributions of the embedding energy term and the pair potential term. Some properties may be determined mainly by the pair potential, such as the barrier energy in the diffusion of vacancies.<sup>[12]</sup> However, others may be determined by the contributions of the embedding energy and the pair potential, while the effect of the embedding energy may be underestimated, such as the planar fault energies in  $\gamma'$  (Ni<sub>3</sub>Al).<sup>[24]</sup> For the construction of the potentials, it is useful to distinguish the effects of the two energy terms on the properties of the materials. The contribution of the embedding energy to the SFE of the Ni(Co, Al) random solid solution is calculated with the present potential and shown in Fig. 4(b). It can be seen from Fig. 4(b) that the embedding energy term contributes little to the SFE of pure  $\gamma$ (Ni). The contribution of the embedding energy term to the SFE ( $E_{\text{SF}}^{\text{embed}}$ ) increases with increasing concentrations of Co and Al. The ratio of  $E_{\text{SF}}^{\text{embed}}$  to the SFE of Ni(Co, Al) ( $E_{\text{SF}}^{\text{alloy}}$ ) is nearly a linear function of  $c_{\text{Co}}$  and  $c_{\text{Al}}$ . In the Ni(12.5 at.% Co, 12.5 at.% Al) random solid solution,  $E_{\text{SF}}^{\text{embed}}/E_{\text{SF}}^{\text{alloy}}$  is greater than 1/2. Therefore, the embedding energy term in the present potential has an important effect on the SFE of the condensed Ni(Co, Al) random solid solution. The SFEs of the Ni(Al) random solid solutions are calculated with the present potential, the Mishin potential,<sup>[48]</sup> and the Voter–Chen potential.<sup>[49]</sup> The calculated results are shown in Fig. 5. It can be seen from Fig. 5 that the decrease in the SFEs upon adding Al is larger for the Mishin and the Voter–Chen potentials than that for the present potential in the Ni(Al) random solid solution with the same  $c_{\text{Al}}$ . The effect of the embedding energy term on the SFE in the present potential is larger than in the Mishin and the Voter–Chen potentials. It has been shown that the effect of the embedding energy term in the alloy is related to the atomic electron densities. The parameter  $s$  in Eq. (4) should be considered in the fitting of the potentials of alloys.<sup>[24]</sup> The embedding energy can include the energy contributions that are due to charge transfer between the background electron gas and the embedded atom, which is not considered in the potentials based on the tight-binding method.<sup>[50]</sup> The background or host electron density in the interatomic potential based on the effective-medium theory<sup>[51]</sup> is defined as  $\rho_i = \langle \sum_{j \neq i} f_j(r) \rangle_{\Omega_i}$ , where  $f_j(r)$  is the atomic electron density from the neighboring atom of atom  $i$ , and the angle bracket denotes the average over the Wigner–Seitz cell ( $\Omega_i$ ) of atom  $i$ . Therefore, the atomic electron density of the atom that loses electrons should have a larger tail, so the host electron densities of the neighboring atoms are increased. In the alloy potentials, the parameter  $s$  in Eq. (4) has the effect of adjusting the tail of the atomic electron density. The electron density difference for  $L1_2$ -Ni<sub>3</sub>Co calculated using Dmol3 with a spin-unrestricted mode and the GGA for the exchange correlation functional is shown in Fig. 6. The electron density dif-

ference is given by subtracting the electron density of isolated atoms from the total electron density. The charge partitioning between Ni and Co given by the Hirshfeld method<sup>[52]</sup> is also shown in Fig. 6. It can be seen from Fig. 6 that the electrons transfer from Co to Ni. The host electron densities calculated with the present potential for the Ni and Co atoms are  $\rho_{\text{Ni}}/\rho_{\text{e}}^{\text{Ni}} = 1.71$  and  $\rho_{\text{Co}}/\rho_{\text{e}}^{\text{Co}} = 0.37$ , respectively. If the equilibrium host electron density of monoatomic metal in EAM

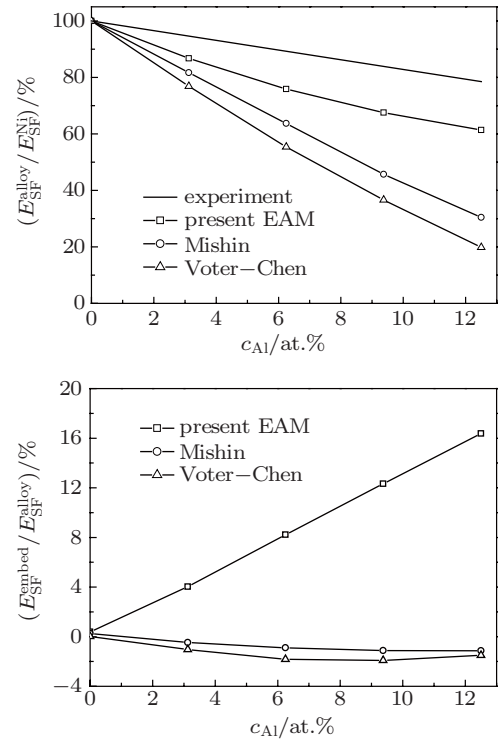


**Fig. 5.** (a) The stacking fault energies of Ni(Al) random solid solutions as a function of the concentration of Al calculated with the present Ni–Al potential, the Mishin potential,<sup>[48]</sup> and the Voter–Chen potential,<sup>[49]</sup> here compared with the experimental values. (b) The contributions of the embedding energy term to the stacking fault energies for the three potentials, where  $E_{\text{SF}}^{\text{Ni}}$  and  $E_{\text{SF}}^{\text{alloy}}$  are the SFEs of the  $\gamma$ (Ni) and Ni(Al) random solid solutions, respectively.

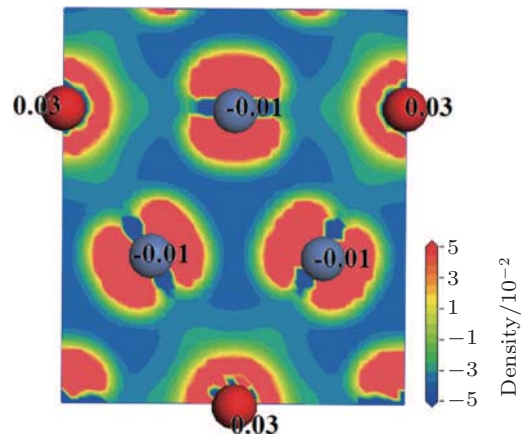


**Fig. 6.** (color online) Electron density variation in the (111) plane of  $L1_2$ -Ni<sub>3</sub>Co. The blue and red balls denote Ni and Co atoms, respectively. The charge partitioning between Ni and Co given by the Hirshfeld method is shown on the atoms.

corresponds to the neutral electron density in first-principles, the conditions of  $\rho_{\text{Ni}}/\rho_{\text{e}}^{\text{Ni}} > 1$  and  $\rho_{\text{Co}}/\rho_{\text{e}}^{\text{Co}} < 1$  in EAM are consistent with the electron transfer from Co to Ni in first-principles.

### 3.4. The effect of Co on the cross-slip activation energy of $\gamma(\text{Ni})$

A screw dislocation in fcc metals dissociates into two partial dislocations separated by a stacking fault. The SFE of  $\gamma(\text{Ni})$  can be decreased by alloying Co, and the width of the stacking fault is increased. The creep resistance of Ni-based solid solutions is usually related to the cross-slip and the climb processes of the dislocations.<sup>[53]</sup> To study the effects of Co on the cross-slip process in  $\gamma(\text{Ni})$  and avoid the influence of variations in the width of the stacking fault in the random solid solution, four homogeneous solid solutions are used in the simulation of the cross-slip process. In the homogeneous solid solutions, the distances between Co atoms are equal. The homogeneous solid solutions are constructed based on a  $2 \times 2 \times 2$  fcc-Ni(Co) supercell containing 32 atoms. The cross-slip model is constructed by periodically repeating the  $2 \times 2 \times 2$  fcc-Ni(Co) supercell, and the concentrations of Co in the four supercell models are 3.1 at.%, 6.3 at.%, 9.4 at.%, and 12.5 at.%, respectively. The SFEs of the homogeneous Ni(Co) solid solutions on the (111) plane are shown in Fig. 7(a), compared with the SFEs of random solid solutions. It can be seen from Fig. 7(a) that the SFEs from the homogeneous Ni(Co) solid solution models are in agreement with those from the random Ni(Co) solid solution models. The cross-slip model is constructed in a cylindrical cell based on the repeated  $2 \times 2 \times 2$  fcc-Ni(Co) supercell. The cylindrical cell has a diameter of 14.4 nm and a length of 14.9 nm. This model contains 258420 atoms. The  $x$  and  $y$  axes are along the  $[12\bar{1}]$  and  $[\bar{1}11]$  directions, respectively, with free boundary conditions. The  $z$  axis is along the  $[101]$  direction with a periodic boundary condition. The dislocation line is along the  $z$  axis. The initial configuration of a perfect screw dislocation is given by displacing the atoms according to the anisotropic elastic displacement field formula.<sup>[54]</sup> The dissociation of the screw dislocation on  $(\bar{1}11)$  or  $(11\bar{1})$  is given by minimizing the total energies with respect to the atomic position. The cross-slip process of the extended dislocation from the  $(\bar{1}11)$  plane to the  $(11\bar{1})$  plane is simulated using the nudged elastic band (NEB) method<sup>[55,56]</sup> and the molecular dynamics software LAMMPS.<sup>[57]</sup> The cross-slip activation energy is the maximum value of the energies in the minimum energy path. The cross-slip activation energies are shown in Fig. 7(b). It can be seen from Fig. 7(b) that the cross-slip activation energies increase with increasing  $c_{\text{Co}}$ . The cross-slip process can be hindered by alloying with Co. Thus, the creep properties that are controlled by the cross-slip process can be improved in Ni(Co) solid solutions.

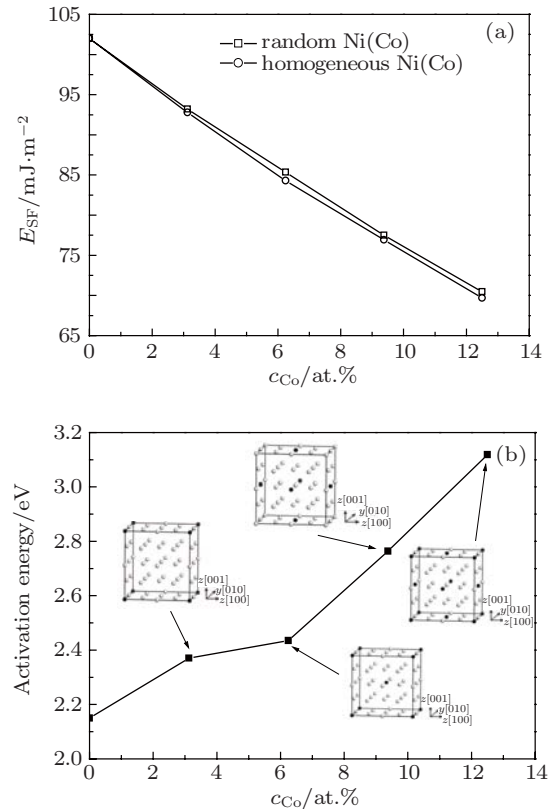


**Fig. 7.** (a) The stacking fault energies of homogeneous Ni(Co) solid solution models compared with the results of Ni(Co) random solid solution models. (b) The cross-slip activation energies in homogeneous Ni(Co) solid solution as a function of the concentration of Co. The insets show the atomic configurations of  $2 \times 2 \times 2$  supercell models containing Co. The white and black balls denote Ni and Co atoms, respectively.

## 4. Summary

A potential suitable for studying the effect of Co on the  $\gamma(\text{Ni})/\gamma'(\text{Ni}_3\text{Al})$  superalloy has been constructed based on experiments and first-principles calculations. The following summarizes our conclusions.

- 1) The stacking fault energies of random Ni(Co, Al) solid solutions decrease with increasing concentrations of Co and Al, which is consistent with the experimental results. The embedding energy term has an important effect on the SFEs of the random Ni(Co, Al) solid solutions, as we learned by considering the charge transfer between different elements.
- 2) The cross-slip activation energies of  $\gamma(\text{Ni})$  are increased by alloying with Co, which implies that the creep resistance of the  $\gamma(\text{Ni})$  may be improved by the addition of Co.

## Acknowledgment

The simulations were carried out on the “Explorer 100” cluster system of Tsinghua National Laboratory for Information Science and Technology, China.

## References

- [1] Reed R C 2006 *The Superalloys: Fundamentals and Applications* (Cambridge: Cambridge University Press)

- [2] Murakami H, Yamagata T, Harada H and Yamazaki M 1997 *Mater. Sci. Eng. A* **223** 54
- [3] Reed R C, Tao T and Warnken N 2009 *Acta Mater.* **57** 5898
- [4] Sato J, Omori T, Oikawa K, Ohnuma I, Kainuma R and Ishida K 2006 *Science* **312** 90
- [5] Zhu T and Wang C Y 2005 *Phys. Rev. B* **72** 014111
- [6] Kohler C, Kizler P and Schmauder S 2005 *Mater. Sci. Eng. A* **400–401** 481
- [7] Xie H X, Wang C Y and Yu T 2009 *Modelling Simul. Mater. Sci. Eng.* **17** 055007
- [8] Wu W P, Guo Y F, Wang Y S, Mueller R and Gross D 2011 *Phil. Mag.* **91** 357
- [9] Liu Z G, Wang C Y and Yu T 2013 *Modelling Simul. Mater. Sci. Eng.* **21** 045009
- [10] Daw M S and Baskes M I 1983 *Phys. Rev. Lett.* **50** 1285
- [11] Daw M S and Baskes M I 1984 *Phys. Rev. B* **29** 6443
- [12] Mishin Y, Farkas D, Mehl M J and Papaconstantopoulos D A 1999 *Phys. Rev. B* **59** 3393
- [13] Wang T M, Wang B Y, Ju X, Gu Q, Wang Y X and Gao F 2001 *Chin. Phys. Lett.* **18** 361
- [14] Wang Z K, Wu Y Q, Shen T, Liu Y H and Jiang G C 2011 *Acta Phys. Sin.* **60** 086105 (in Chinese)
- [15] Yuan X J, Chen N X, Shen J and Hu W Y 2010 *J. Phys.: Condens. Matter* **22** 375503
- [16] Yuan X J, Chen N X and Shen J 2011 *Chin. Phys. Lett.* **28** 123402
- [17] Yuan X J, Chen N X and Shen J 2012 *Chin. Phys. B* **21** 053401
- [18] Zhang C H, Huang S, Shen J and Chen N X 2012 *Chin. Phys. B* **21** 113401
- [19] Xie Q, Xu W and Huang M 1995 *Chin. Phys. Lett.* **12** 12
- [20] Oh D J and Johnson R A 1989 *J. Nucl. Mater.* **169** 5
- [21] Pasianot R and Savino E J 1992 *Phys. Rev. B* **45** 12704
- [22] Jiang M, Oikawa K and Ikeshoji T 2005 *Metall. Mater. Trans. A* **36** 2307
- [23] Igarashi M, Khantha M and Vitek V 1991 *Philos. Mag. B* **63** 603
- [24] Du J P, Wang C Y and Yu T 2013 *Modelling Simul. Mater. Sci. Eng.* **21** 015007
- [25] Banerjee A and Smith J R 1988 *Phys. Rev. B* **37** 6632
- [26] Delley B 1990 *J. Chem. Phys.* **92** 508
- [27] Delley B 2000 *J. Chem. Phys.* **113** 7756
- [28] Mishin Y, Mehl M J and Papaconstantopoulos D A 2002 *Phys. Rev. B* **65** 224114
- [29] Born M and Huang K 1954 *Dynamical Theory of Crystal Lattices* (Oxford: Clarendon)
- [30] Van Midden H J P and Sasse A G B M 1992 *Phys. Rev. B* **46** 6020
- [31] Peng P, Soh A K, Yang R and Hu Z Q 2006 *Comput. Mater. Sci.* **38** 354
- [32] Wang Y J and Wang C Y 2008 *J. Appl. Phys.* **104** 013109
- [33] Kresse G and Hafner J 1993 *Phys. Rev. B* **48** 13115
- [34] Kresse G and Furthmüller J 1996 *Phys. Rev. B* **54** 11169
- [35] Rose J H, Smith J R, Guinea F and Ferrante J 1984 *Phys. Rev. B* **29** 2963
- [36] Barrett C S and Massalski T B 1980 *Structure of Metals* (3rd edn.) (Oxford: Pergamon) p. 626
- [37] Kittel C 1976 *Introduction to Solid State Physics* (5th edn.) (New York: Wiley)
- [38] Brandes E A and Brook G B (ed.) 1992 *Smithells Metal Reference Book* (7th edn.) (Oxford: Clarendon) pp. 15–16
- [39] De Boer F R, Boom R, Mattens W C M, Miedema A R and Niessen A K 1988 *Cohesion in Metals: Transition Metal Alloys* (Amsterdam: North-Holland)
- [40] Korner A and Karnthaler H P 1983 *Phil. Mag. A* **48** 469
- [41] Neumeier S, Pyczak F and Göken M 2008 *Superalloys 2008* (Warrendale: The Minerals, Metals&Materials Society) p. 109
- [42] Carroll L J, Feng Q, Mansfield J F and Pollock T M 2007 *Mater. Sci. Eng. A* **457** 292
- [43] Nathal M V and Ebert L J 1985 *Metall. Trans. A* **16** 1849
- [44] Davies C K L, Nash P and Stevens R N 1980 *J. Mater. Sci.* **15** 1521
- [45] Wang Y J and Wang C Y 2009 *Mater. Res. Soc. Symp. Proc.* 1224 FF05-31
- [46] Xie X S, Chen G L, Mchugh P J and Tien J K 1982 *Scripta Metall.* **16** 483
- [47] Schönfeld B, Reinhard L, Kostorz G and Bührer W 1997 *Acta Mater.* **45** 5187
- [48] Mishin Y 2004 *Acta Mater.* **52** 1451
- [49] Voter A F and Chen S P 1987 *Mater. Res. Soc. Symp. Proc.* **82** 175
- [50] Carlsson A E 1990 *Solid State Physics* **43** 1
- [51] Jacobsen K W, Nørskov J K and Puska M J 1987 *Phys. Rev. B* **35** 7423
- [52] Hirshfeld F L 1977 *Theor. Chim. Acta* **44** 129
- [53] Nabarro F R N and de Villiers H L 1995 *The Physics of Creep* (London: Tylor & Francis Ltd)
- [54] Hirth J P and Lothe J 1982 *Theory of Dislocations* (New York: John Wiley & Sons)
- [55] Henkelman G, Uberuaga B P and Jónsson H 2000 *J. Chem. Phys.* **113** 9901
- [56] Henkelman G and Jónsson H 2000 *J. Chem. Phys.* **113** 9978
- [57] Plimpton S 1995 *J. Comput. Phys.* **117** 1